Experimental Demonstration of a Metro Area Network with Terabit-capable Sliceable Bitrate Variable Transceiver using Directly Modulated VCSELs and Coherent Detection

J. M. FABREGA[1], F. J. VÍLCHEZ[1], M. SVALUTO MOREOLO[1], R. MARTÍNEZ[1], A. QUISPE[1], L. NADAL[1], R. CASELLAS[1], R. VILALTA[1], R. MUÑOZ[1], C. NEUMEYR[2], S. Y. LEE[3], J. U. SHIN[3], H. D. JUNG[3], G. MARIANI[4], R. HEUVELMANS[4], A. GATTO[5], P. PAROLARI[5], P. BOFFI[5], N. M. TESSEMA[6], N. CALABRETTA[6], D. LARRABEITI[7], AND J. P. FERNÁNDEZ-PALACIOS[8]

[1] *Centre Tecnologic de Telecom. de Catalunya (CTTC/CERCA), Castelldefels, Spain*
[2] *Vertilas GmbH, Garching bei Munchen, Germany*
[3] *Electronics and Telecommunications Research Institute (ETRI), Daejeon, Korea*
[4] *Effect Photonics B.V., Eindhoven, Netherlands*
[5] *Politecnico di Milano, Milan, Italy*
[6] *Technical University of Eindhoven (TUE), Eindhoven, Netherlands*
[7] *Universidad Carlos III de Madrid, Madrid, Spain*
[8] *Telefónica Global CTO, Madrid, Spain*
[*] *Corresponding author: jmfabrega@cttc.es*

Compiled January 2, 2023

Disaggregation in optical networks is particularly relevant to be considered for the deployment of 5G services and towards the support of 6G. Particularly in the metro area network (MAN), this is specially crucial as well as the adoption of suitable photonic technologies enabling dense integration to design a sustainable network architecture. Furthermore, to dynamically allocate the ever increasing traffic, supporting multi-Terabit capacity, an optimal usage of the available resources is key, properly exploiting the multiple dimensions (including the spectral and spatial ones), with programmable and adaptive data plane solutions. In this work, we assess the capabilities of a disaggregated metro area network that relies on new photonic devices, node architectures, and sliceable bandwidth/bitrate variable transceivers, approaching wavelength division multiplexing and space division multiplexing. A hierarchical network topology is attained and the feasibility of a cross-hierarchy optical continuum is demonstrated. In fact, we experimentally demonstrate the successful transmission of multi-Tb/s capacity across multiple nodes corresponding to different hierarchy levels, that have different implementation schemes and support different technologies. For the top tier hierarchy level nodes, we demonstrate the transmission of up to 8×11=88 spatial/spectral channels, for a total capacity of 1.676 Tb/s, employing a node architecture able to handle up to 2560 spatial/spectral channels at different aggregation levels and granularities.

http://dx.doi.org/10.1364/ao.XX.XXXXXX

1. INTRODUCTION

Telecom operators are fostering disaggregation in optical network systems because it enables a vendor lock-in-free upgrade of network components [1]. This is particularly relevant in the access and metro area networks (MAN), where the progressive deployment of 5G is expected to require major changes of installed capacities. Moreover, operators are seeking for photonic technologies suitable to be integrated in those disaggregated architectures able to allocate the underlying bandwidth wherever needed with unprecedented flexibility. The ultimate goal is to properly manage high traffic variances and high capacity demands by means of (super-)channels at low cost and high power efficiency [2]. This brings the need to explore novel network architectures and photonic technologies [3].

In the framework of EU-H2020 PASSION project, we approached a disaggregated MAN architecture with different hierarchical levels (HLs), ranging from those close to the edge (HL4) up to the core (HL1 and HL2) [4]. Lower level metro-aggregation nodes (HL4, aggregating traffic from edge nodes at HL5) handle only spectrum, are typically interconnected by rings and are based on simple wavelength blockers [5]. HL3 nodes are transit switches with 25 GHz granularity (using wavelength selective switches, WSSs) enabling all-optical routing of optical channels from HL4 nodes toward the core, where most of the MAN traffic is originated, either at service nodes (HL2, usually hosting CDN caches) or at WAN nodes (HL1). HL2 and HL1 nodes, making up the MAN core, are usually interconnected in a mesh topology, adopt specific photonic switching technologies to manage the spectral and spatial dimensions [6] and the traffic may be forwarded at the IP layer or further be routed at the photonic layer.

In terms of photonic transmission technologies, we propose the use of photonic integrated circuits (PICs) and arrays of vertical cavity surface emitting lasers (VCSELs). The goal is building fully programmable sliceable bandwidth/bitrate variable transceivers (S-BVTs) using directly modulated VCSELs and integrated coherent receivers to provide a solution with reduced cost, power consumption and carbon footprint [3].

The programmability of the transport domain including S-BVTs (i.e., VCSELs and coherent receivers) along with the optical switches is automatically handled by a dedicated and centralized software-defined networking (SDN) controller. Thereby, the controller takes over of processing incoming connection service requests demanded by an external application/system and arriving through a defined applications programming interface (API, i.e., a northbound interface). These requests specify the connection endpoints (i.e., source and destination) and the required bandwidth. Then, the controller triggers and coordinates a set of control operations and functions to eventually set up the connection service. Firstly, it is selected/computed the path (i.e., nodes and links) and resources (i.e., VCSELs, coherent receivers, frequency slots) that allow fulfilling the connection demands [7, 8]. This computation is done by a routing and spectrum assignment (RSA) algorithm. The aim of the algorithm is to output the available resources that fulfill the connection needs (i.e., bandwidth). Secondly, the SDN controller communicates with the agents governing each transport device to query the allocation of the selected resources (i.e., RSA output). To do that, defined APIs between the controller and the device agents are used to: *i)* retrieve information about the status of the devices and their resources i.e., unused VCSELs and coherent receivers, and available optical spectrum in the links; *ii)* configure the resource allocation and de-allocation. These APIs entail the design and implementation of data models which allow the device agents abstracting relevant resource information needed by the SDN controller to serve incoming optical connection requests.

In this paper, we demonstrate the performance achievable with the PASSION network approach. In fact, this is an extension of the conference paper [9], where we deployed a 5-node network path including HL4, HL3 and HL2 nodes, featuring flexible spectral and spatial switching and covering up to 110 km-distance including a 25 km 19-core multicore fiber (MCF). Here, we further describe essential hierarchical network design aspects leading to relevant savings in terms of number of transceivers at intermediate levels and provide a complete description of the S-BVTs used. These VCSEL-based S-BVTs are the ones integrated in the experimental setup, that are used for validating the transmission of 11 spectral channels densely spaced (25 GHz) over 8 different cores through that network. In addition, the SDN control programmability to configure HL3/HL2 nodes is assessed.

The paper is structured as follows. First, section 2 provides a state of the art in order to contextualize the investigations reported in this paper. Next, in section 3 the proposed network scenario is detailed and discussed, providing the details of the different network elements. Section 4 details the SDN controller architecture with special emphasis on the APIs used to configure the transport network elements. Section 5 deals with the experimental network setup, whereas section 6 reports the results of the experiments. Finally, conclusions are drawn in section 7.

2. PRIOR ART

This paper comes after developing and putting together many different technologies that take a step further over the actual state of the art.

The first is the incorporation of direct modulation lases (DMLs) into the transmission system. This option is quite appealing because, the combination of external Mach-Zehnder modulator(s) and tunable laser source(s) is a more costly solution with more flexibility and performance when compared to DMLs. In terms of cost, footprint, and power consumption, DMLs outperform external modulated laser (EML) solutions. This makes DMLs an appealing option for achieving high-speed performance, particularly when combined with advanced modulation formats and required chip floor space [10]. In fact, in [10], a comparison is offered at varied rates, bandwidth, and spectral efficiency, demonstrating that the penalty due to DML nonlinearity may be insignificant in the case of selecting particular modulation schemes over others. Indeed, the achievable reach is important in determining if DML is a viable alternative. In this sense, coherent reception improves performance while extending the reach when compared to direct detection. Nevertheless it comes at increased cost/complexity because it requires a local oscillator at the receiver side, preferably tunable over a given optical band.

VCSELs offer lower manufacturing costs than other DML choices (e.g., distributed feedback lasers) due to the ease of testing (thanks to vertical emission), allowing for mass production. When compared to edge emitting laser systems, optimized structures in indium phosphide enable operation at long wavelengths with low threshold current and operating voltage, resulting in significantly reduced power consumption. Less than 10 mW power consumption has been observed for very high bandwidth VCSELs (up to 22 GHz) [11]. These characteristics make this option particularly appealing for usage in both the access and MAN segments of (SDN-controlled) optical networks [12].

Even though VCSEL technology is usually considered for short reach and low bitrate applications, mainly at short wavelengths, its potential operation in the third window has been explored for targeting access and metro networks, as well as applications at 100 Gb/s and beyond [13–15]. In particular, the evolution of technology towards tunable and large-bandwidth (>18 GHz) VCSELs [11, 16], which can be directly modulated with advanced modulation formats, including orthogonal frequency division multiplexing (OFDM), opens up new horizon for its adoption, even for the design of programmable transceivers [7]. High-speed operation and higher modulation bandwidth are achieved by a suitable structure design reducing the parasitic effects and the optical cavity length [11, 16]. It is worth men-

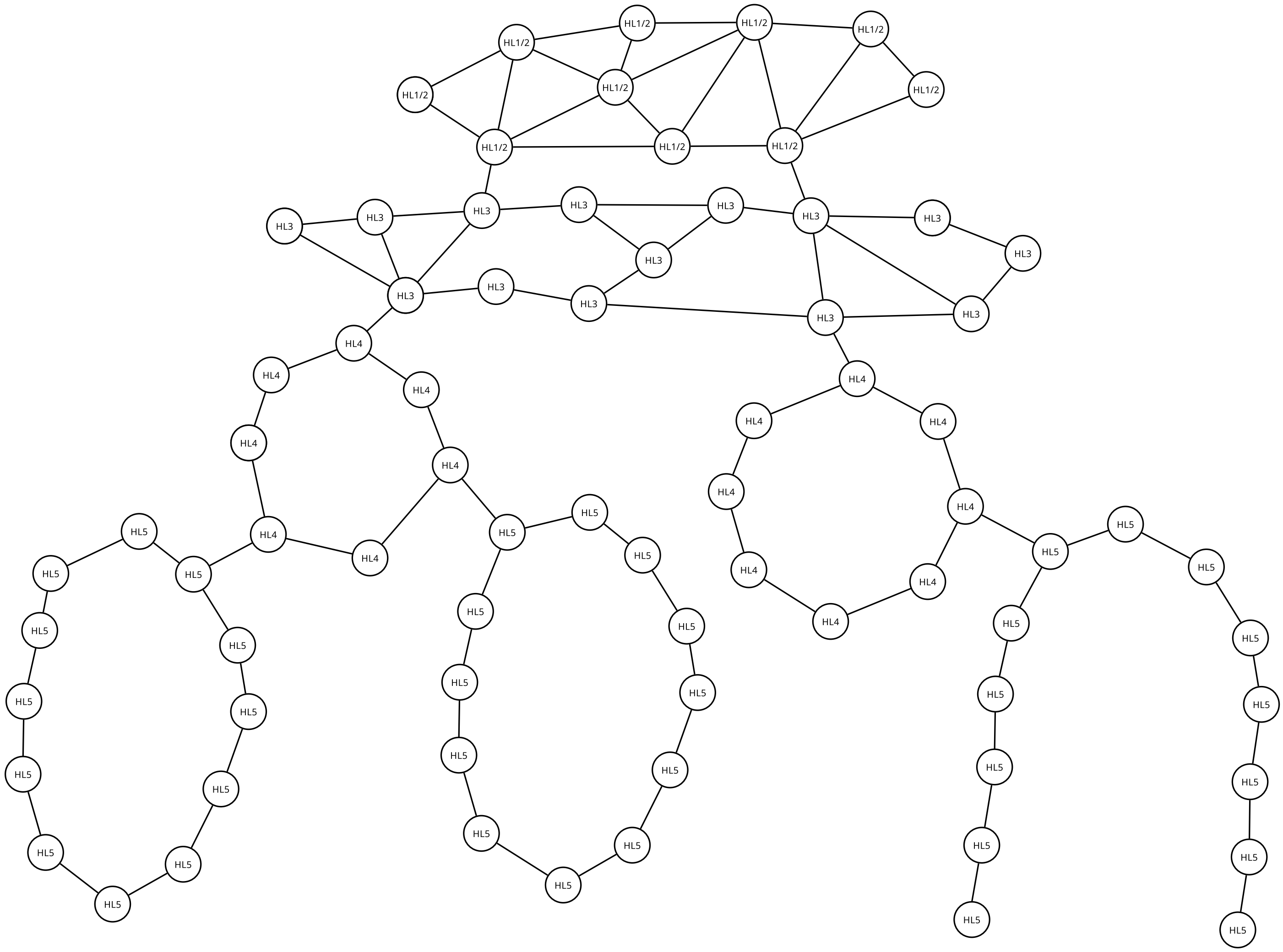

Fig. 1. Sample conceptual topology scheme of the network.

tioning that discrete multi-tone (an OFDM variant) can be a promising solution to target 1T-class transceivers, taken into account the advances in CMOS technology, towards a reduction of the power consumption required by this modulation format compared to others (such as PAM-4) [10].

Regarding the node architectures, in our case we are implementing different subsystems that lead to a modular reconfigurable add/drop multiplexer (ROADM). The most challenging are those that can incorporate SDM switching. The key choice for transparently switching SDM systems is a modular ROADM with color-less, direction-less, and contention-less (CDC) features. Numerous efforts have been done, approaching such ROADMs [17–19]. The key issues in CDC-ROADM are the increasing cost and complexity of the (wavelength and space) switching subsystems when increasing the traffic and, thus, the number of wavelength channels. This is worsened even further when approaching SDM, generally implemented by including multi-core fibers. As a result, new, efficient, and scalable ROADM for SDM systems based on modular architectures and low-cost photonic integrated wavelength and space switching are being researched [17, 20]. In PASSION, the approach is to have a unique modular ROADM architecture for SDM that includes a photonic space switch with express (bundled traffic) and add/drop ports, photonic integrated wavelength selective switches (WSS) aggregation/disaggregation capabilities for merging/dropping network traffic, and a photonic integrated multi-cast switch [5].

One of the core parts of the ROADMs, are the optical switches. In this sense, commercial wideband optical switches are based on micro-electro-mechanical system (MEMS) and piezo-electric technologies. However, despite their high performance, these devices are large and costly to mass produce due to their intricate construction. As a result, PIC-based optical switches are appealing because they can provide mass repeatability, reduced cost, smaller size, and stability. Several PIC switches on silica have been proposed that use the thermo-optic effect and have a mild loss characteristic [21, 22]. The main disadvantages of those switches are the high polarization dependent operation (the polarization diversity doubles the device components and requires strict control of the polarization), wavelength dependent performance and fiber to chip coupling losses, and high power consumption due to low thermo-optic coefficient. PIC polymer thermo-optic switch using total-internal-reflection (TIR) effect has the potential to operate as wideband optical switch with polarization and wavelength independent operation, data rate transparent and lower power consumption [23].

3. CONCEPT

A. Network

In this paper we approach a disaggregated metro area network architecture featuring different hierarchy levels, as shown in figure 1.

Taking a bottom-up approach, HL5 is the lowest level of such a network, making up the real edge of the MAN facing the access segment. HL5 nodes can be small central offices (COs) hosting FTTH optical line terminals (OLTs), among other access equipment or simply 4G/5G base stations (BSs). The typical topology interconnecting HL5 nodes is a large ring not necessarily optical, i.e. forwarding and aggregation of traffic takes place at the packet layer, either IP/ethernet, MPLS-TP or simply metro ethernet. All the traffic collected by HL5 nodes is aggregated at one HL4 node (or two, in redundant settings). HL4 nodes aggregate this traffic at the packet layer and, in the PASSION architecture, this traffic is all-optically transported to the core (HL2/1) optically by-passing HL3 routers, with an important cost saving in terms of O/E/O conversions, packet forwarding and carbon footprint at HL3. HL4 are normally big COs expected to manage up to Tb/s in the next years. The router of the HL4 node aggregates the traffic from a number of HL5 rings and forwards the traffic to the core by means of an S-BVT. HL4s are interconnected with either a ring or horseshoe topology at the physical layer; but normally the logical IP layer is configured as to provide dual connectivity to two different HL3 nodes or, as proposed in PASSION, with dual dynamic bandwidth-variable all optical links to two different HL2/HL1 nodes. As a consequence, HL3 nodes are mainly devoted to traffic aggregation/distribution at the optical layer. The routers hosted by these transit nodes do not need to handle the whole traffic directed to/from the core; they just need to deal with the aggregation of local traffic and non-hierarchical traffic. According to statistics collected by Telefonica, non-hierarchical traffic accounts for 10% of the total traffic. The rest corresponds to CDN traffic and Internet Exchange Points (IXP) peering traffic (coming from HL2 nodes, or in some cases, HL3 nodes) and non-cacheable Internet content traffic (coming from HL1 nodes). Therefore, HL2 -hosting services such as IP telephony and IPTV- and HL1 -hosting WAN connectivity- are the source or destination of the majority of the traffic of the MAN. The PASSION approach tries to leverage such circumstance.

Please note that in this conceptual approach the only foreseen grey interfaces of the network are located at HL5 and HL4, while the other hierarchy levels are expected to feature all optical aggregation and distribution of traffic. This is important, as it paves the way towards the implementation of the so-called optical continuum. Therefore, in terms of optical connectivity, the most challenging case is when we tackle connections between HL4 and HL1/2 nodes, where the optical channel is assigned at the source HL4 and optically transported to any destination node at HL2 or HL1. In this case optical paths are long (in distance) as well as a complex traffic accommodation is required, taking into account the available wavelengths depending on the destination HL1/2 node. In fact, we expect to cover paths of up to 200 km and up to 10 hops [24].

B. Network nodes

Regarding the design of network nodes, different architectures are envisioned depending on the hierarchy level. The nodes corresponding to lower level aggregation nodes (HL4, aggregating traffic from edge nodes at HL5) are numerous and only able to handle spectrum. Therefore, they can be based on simple wavelength blockers employing semiconductor optical amplifiers (SOAs) [5]. HL3 nodes are transit switches and are expected to feature a minimum of 25 GHz granularity for enabling the desired all-optical routing from HL4 nodes to HL2/1. Therefore, a possible implementation is based on common wavelength selective switches (WSSs), e.g. compliant with ITU-T flexgrid. HL2/1 nodes interfacing the core network adopt specific photonic switching technologies to support multiple functionalities and granularities while handling spectral and spatial dimensions [6]. Importantly, these nodes feature an initial switching stage, that can be implemented in polymer PICs which has the advantage of low loss, low cost, and low power consumption [23]. This polymer PICs switch is a thermo-optic matrix switch with a TIR switching element and packaged with BGA bonding technology to minimize metal wiring on the polymer material.

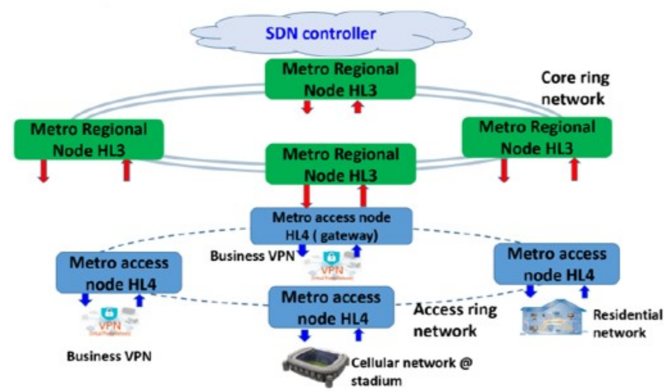

Fig. 2. SDN enabled Metro core and metro access network architecture

A typical example of a deployed metro-core and access network scenario is shown in Fig. 2. The HL3 switching nodes are connected to access network mainly constituted by a network of Hierarchical level-4 (HL4) nodes. The HL4 nodes are the closest to the end users and may be connected in a different topologies, a ring topology can be an example as presented in Fig. 2. The HL4 nodes can for instance support traffic for business VPN, residential network connectivity and cellular networks. The photonic WDM switches embedded in HL3 and HL4 nodes enable leveraging wavelengths to traffic conditions where they are most needed temporarily, for instance a cellular network in a stadium during sporting events.

C. Transceivers

The transceivers envisioned to be used in this concept are modular programmable S-BVTs based on VCSEL technology and dense photonic integration [25]. Thus, according to the required traffic to be supported over an established lightpath, the corresponding VCSEL source(s) operating at the appropriate wavelength(s) are enabled/disabled by a SDN controller for a dynamic path and/or capacity adaptation. Specifically, the SDN paradigm enables to suitable reconfigure the transceiver according to the network requirements by the implementation of SDN agents. Each S-BVT is composed of BVT transmission/reception pairs whose inputs/output are appropriately aggregated/disaggregated e.g. using a wavelength multiplexing/demultiplexing stage [3].

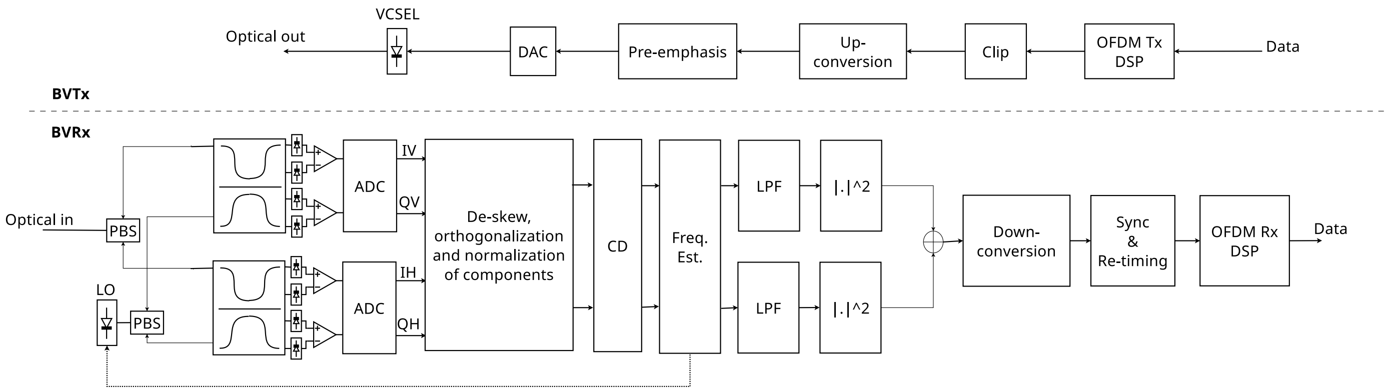

Fig. 3. Inner scheme of each BVT. BVTx: Bandwidth/bitrate variable transmitter; BVRx: Bandwidth/bitrate variable receiver.

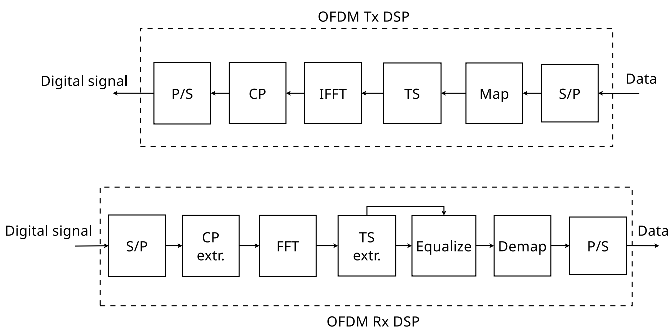

Fig. 4. Scheme of OFDM DSP.

Fig. 3 shows the details of the basic BVT pair enabling the whole concept. This is based on intensity modulation and coherent reception and employs OFDM modulation. Details are as follows.

At the transmitter, incoming data are first processed at the OFDM digital signal processing (DSP) stage in order to generate a digital OFDM waveform, as shown in Fig. 4. So, data are parallelized and mapped into the corresponding M-level quadrature amplitude modulation (QAM) constellation. Adaptive bit/power loading can be implemented for either optimizing the performance at a given capacity, or optimizing capacity at a given performance. For example, the rate adaptive version of the Levin-Campello algorithm [26] can be used in order to test the maximum capacity that the BVT can offer. Then, training symbols (TS) are included for performance monitoring and extracting the channel response at the receiver side. The resulting symbols feed an inverse fast Fourier transform (IFFT). Afterwards, a cyclic prefix (CP) is added and the obtained OFDM symbols are then serialized and upsampled. The digital OFDM signal is clipped and upconverted to an intermediate frequency of half of its bandwidth by mixing with a digital oscillator. The resulting signal is pre-emphasized and converted to the analog domain by a digital to analog converter (DAC). This signal drives the VCSEL.

The VCSEL bandwidth might be rather limited when compared to common external modulation. So, the edge of the frequency response of the laser is expected to be smoothly decreasing when increasing the frequency. Therefore, adaptive modulation is very much indicated in this case, since it enables to locally use constellations featuring low bits per symbol. Also, pre-emphasis filtering equalizes the intensity response of the laser by giving and increased gain at high frequencies with respect to low frequencies.

VCSELs are expected to be temperature-controlled. In case fabrication tolerances could not be compensated by temperature control, the eventual wavelength mismatch can be compensated by the control plane as a flexgrid approach used and beat unit for setting up the channels in the network.

In order to improve the transmission performance, an optical bandpass filter can be placed after the optical output for obtaining an optical single side band (SSB) signal. This function can be implemented by the flow aggregator, which is typically a wavelength multiplexer with filtering capabilities.

At the receiver, an optoelectronic front-end based on coherent reception is proposed. The received signal is appropriately interfered in a polarization-diverse 90-degree hybrid by a local laser, which acts as a local oscillator (LO). At the output of the hybrid(s), four balanced detection pairs drive a couple of two-channel analog to digital converters (ADCs). The LO is set at a frequency so that the electrical signals are centered in baseband, even when they feature SSB. In that case the bandwidth of the ADCs can be minimized thanks to the fact that an optical SSB signal features a reduced bandwidth. The digitized in-phase and quadrature (IQ) signals are first de-skewed, orthogonalized and normalized in order to optimally combine them, obtaining a proper complex representation of the received signal. Afterwards, chromatic dispersion (CD) is compensated, by employing a suitable digital filter, and the frequency difference between LO and received signal is estimated. This value is then driving the LO in order to compensate the laser frequency drift and obtain an accurate baseband representation of the received signal. A digital low pass filter (LPF) is applied and the square modulus function is applied in order to obtain a representation of the power of the received signal per polarization. These signals are added and the resulting OFDM signal is downconverted to baseband. Then, a sync and retiming (downsampling) procedure is applied to obtain a suitable baseband OFDM signal. Finally, the baseband OFDM signal is demodulated following the reversal of the OFDM modulation above described.

De-skew, orthogonalization and normalization of the IQ components is key for the performance of any coherent receiver. Of course, when employing an integrated receiver front-end is more advantageous, since delays in the different paths of the balanced detectors can be appropriately designed and manufactured.

One of the key modules of the receiver is the LPF. This filter is specifically designed to avoid unwanted mixing products between LO and received signals, while rejecting as much noise

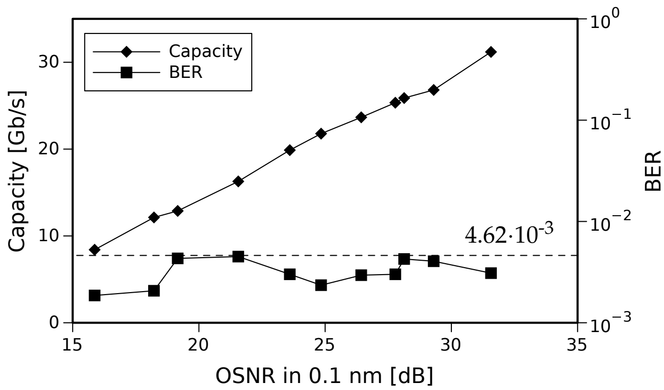

Fig. 5. Capacity vs OSNR for the back to back.

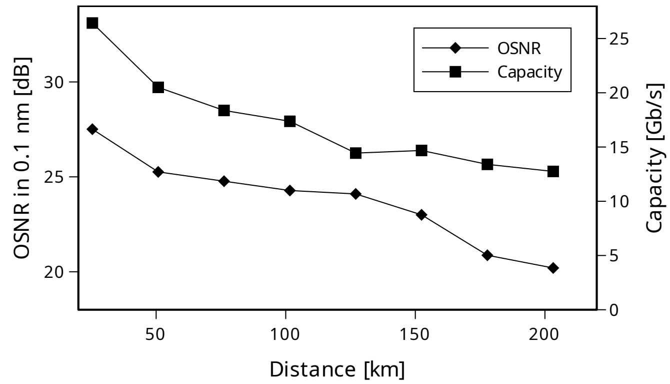

Fig. 6. Capacity and OSNR after transmission for several distances.

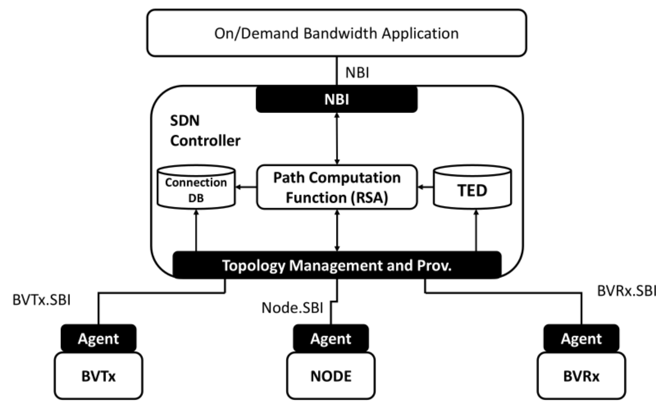

Fig. 7. SDN controller building blocks and APIs.

as possible. Therefore, its response is expected to feature sharp edges and a rather limited bandwidth. So, the LO needs to be able to provide an accurate frequency difference between LO and received signals.

In our case, we have implemented the BVT units using 10G VCSELs and offline DSP. The OFDM signal has been configured to feature 16 Gbaud, centered at 8 GHz. A 4-channel high-speed DAC (up to 64 GSa/s and 13 GHz electrical bandwidth) is used to convert the digital OFDM signals and provide electrical analog signals.

The receiver is an integrated coherent front-end, featuring polarization/phase diversities and a ring cavity laser prototype acting as local oscillator [27]. A real-time digital oscilloscope (running at 50 GSa/s and featuring 20 GHz bandwidth) is used for acquiring the IQ electrical signals corresponding to the two orthogonal states of polarization.

In order to have a first performance metrics of the system, a back-to-back characterization is performed in terms of maximum capacity. For all the results reported, the bit error ratio (BER) obtained is within the range between 10^{-3} and $4.62{\cdot}10^{-3}$, corresponding to the threshold values for a standard hard decision forward error correction (FEC) featuring 7 % overhead [28]. The back-to-back results are shown in Fig.5. There we can observe that the maximum capacity (31.2 Gb/s) is attained for an optical signal to noise ratio (OSNR) value of 31.6 dB and $3.09{\cdot}10^{-3}$ BER. In this case, capacity decreases almost linearly down to 8.41 Gb/s for 15.87 dB OSNR.

Next, we incorporate the transceiver in a recirculating loop. The loop includes a 25.4 km multicore fiber (MCF) and 2 erbium-doped fiber amplifiers (EDFAs). So we can evaluate the performance after distance in steps of 25.4 km and the corresponding OSNR degradation. Results are shown in Fig. 6. There we can see that capacity starts decreasing according to the back-to-back results in terms of capacity/OSNR performance. After 203.2 km, we obtain 20.2 Gb/s and 20.2 dB of OSNR, around 1 dB away with respect to the back-to-back.

4. IMPLEMENTED SDN CONTROLLER ARCHITECTURE

Fig. 7 depicts the architecture of the SDN controller (based on a proprietary CTTC implementation) and their APIs to allow: *(i)* interacting with an external *on-demand bandwidth* application through the northbound interface (NBI); and *(ii)* communicating via the southbound interface (SBI) with the local controllers (i.e., agents) governing each network device, namely, BVTx, BVRx, and the nodes (i.e., optical switches).

The core element of the SDN controller is the path computation function. This handles the spatial and spectral path and resource (i.e., wavelengths/VCSELs) selection and allocation for each incoming connection request. The path and optical resources to be allocated are computed by triggering a RSA algorithm. Basically, the RSA selects those resources that do fulfill the connection requirements (e.g., bandwidth) between a pair of endpoints. Thereby, the RSA algorithm output determines: the VCSELs and optical receivers to be configured (at both BVTx and BVRx), the nodes and links to be traversed, and the optical spectum to be occupied. The used RSA algorithm tailored to the features/constraints imposed by both VCSEL-based BVTx and coherent receivers BVRx was reported by the authors in [29].

The active connection services are stored in the connection database. Thus, the SDN controller handles the lifecycle management of them, i.e., creation, updating, and termination. On the other hand, the traffic engineering database (TED) is a repository to keep track of the status of the underlying transport infrastructure. In other words, the TED has detailed view of the unused/occupied devices at the endpoints (BVTx and BVRx), the unused optical spectrum on every link, as well as the node connectivity, etc. Finally, the NBI and the topology management and provisioning functions allow the communication with the an external application (herein referred to as on-demand bandwidth) and the agents controlling every transport element and device, respectively. Thus, the NBI represents the frontend enabling an on-demand bandwidth application to query the provisioning/updating/termination of connection services, respectively.

On the other hand, the topology management and provisioning entity manages the operations to *i)* retrieve the resource status, and *ii* configure of the underlying transport infrastructure. In light of the presented SDN controller architecture, this fits with a fully disaggregated solution where the controller has a full visibility of the underlying devices within the domain along with the responsability to configure them. That is, the SDN controller does not delegate the optical switching configuration to a dedicated optical line system (OLS) controller manager.

In the following, it is detailed the APIs (workflows and data models) used by the SDN controller to process incoming requests from the on-demand bandwidth application and interact with the underlying transport devices.

A. Workflow and control APIs

Fig. 8 depicts the workflow handled by the SDN controller to process and set up a new connection service queried by the external upper-bound application. The connection request, received over the NBI, is implemented through a REST (`POST`) message (see step 1). The contents are JSON-encoded whose data model (see Fig. 9.a)) describe: the connection (label switched path, lsp) identifier, the ingress BVTx (source), the egress BVRx (destination), the demanded bandwidth in Gb/s units, and the targeted RSA algorithm (objective function, OF).

The connection requests is then served by the path computation function. This firstly steers the TED updating (steps 3-11). To do so, the path computation using the topology management and provisioning block sends REST `GET` messages to both source BVTx and destination BVRx agents to retrieve the status of the VCSELs and coherent receivers, respectively. Additionally, the node agents are also queried to inform about the optical spectrum availability on their links. After the TED is updated, the RSA algorithm is executed fulfilling the connection demands (i.e., step 12). If the RSA computation succeeds, the resulting output specifies the selected frequency slot/s (central frequency - n, and slot width - m) along with the nodes and links to accommodate the connection service. Observe that to meet the connection bandwidth demand, more than one VCSEL and coherent receiver may need to be allocated at the BVTx and BVRx, respectively. In other words, the connection service entails *N* frequency slots (each having its own n and m) which derives on allocating *N* VCSELs and coherent receivers at the source BVTx and destination BVRx.

The workflow continues with the actual resource allocation, i.e., steps 13-20. For the BVTx, a REST `POST` message is sent to BVTx agent. The message contents (JSON-encoded) specify (see Fig. 9.b) the connection id and an array with the frequency slots to be allocated. Each individual array element determines the central frequency (i.e., n) tied to a specific VCSEL, the slot width (i.e., m), a used state boolean to determine whether the resource is to be occupied or released, and other configuration attributes such as the modulation format and FEC. Upon receiving this information, the proprietary agent implementation relies on a GPIB API to de-/activate the selected VCSEL/s. Analogously, the coherent receivers at the BVRx are programmed. To that, the frequency local oscillator parameter (in THz), specified in the Fig. 9.c), is programmed by the BVRx agent into the device via a GPIB API. Finally, for each traversed node, the SDN controller sends a REST (`POST`) message. The message body (Fig. 9.d contains: the connection identifier, the ingress and egress ports, the central frequency (i.e., n) and the slot width (i.e., m). Upon receiving this message, the agent of the node uses the internal APIs (based on TL1 and proprietary implementation) to programm the cross-connections of the frequency slots. A demonstration of the whole SDN controller programming the underlying devices in a transport domain was conducted by the authors in [30].

5. NETWORK EXPERIMENTAL SETUP

The experimental setup is shown in Fig.10. The transmission experiments are based on offline processing implemented in the programmable DSP Tx (DSP Tx 1, DSP Tx 2) modules using Python software, following the steps detailed in section 3C. Adaptive bit/power loading is implemented using the Levin-Campello rate adaptive algorithm in order to test the maximum capacity that the system can offer. As said before, a 4-channel high-speed DAC, running at 64 GSa/s and featuring 13 GHz electrical bandwidth, is used to convert the digital OFDM signals and provide electrical analog signals. The OFDM signals after DAC 1 and DAC 2 feed the corresponding VCSELs (VCSEL1, VCSEL2). VCSEL1 is the actual signal under test, while VCSEL2 is used for generating a set of 10 dummy signals with 25 GHz spacing for emulating the different spectral slices of the S-BVT.

The dummy signals are generated by means of a recirculating frequency shifting technique [31]. There a seed signal (generated after SSB filtering VCSEL2 output) is frequency shifted by the IQ modulator, amplified and re-injected into the modulator, generating a second frequency shifted signal. This process continues until terminated by one of the edges of the optical bandpass filter (OBPF) present in the loop. A couple of three-paddle polarizers are placed in the loop for aligning the state of polarization of the signals with the IQ modulator axes.

The optical signal generated by VCSEL1 is SSB filtered and injected to the network by means of an optical coupler that emulates the add channel operation of an HL4 node. Filtering is performed by a WSS that also includes selected dummy channels suitable for the 100 GHz spacing of the HL4 nodes (see Fig.11a). The signals then traverse a 10 km standard single mode fiber (SSMF) spool that connects to another HL4 node. The latter node performs a pass-through operation by activating the SOA corresponding to the channel in use and connects to a HL3 node by means of a 5 km SSMF spool. The HL4 nodes are implemented by using 100 GHz arrayed waveguide gratings (AWGs) and SOA for wavelength blocking [5] (see Fig.11b). At the HL3 node N2, the 25 GHz-spaced dummy channels are added by means of a 50:50 coupler and transmitted over 2 links of 35 km SSMF in the ADRENALINE testbed [32]. Optical spectra at this point is depicted in Fig.11c. Nodes N2, N3 and N4 are implemented using flexgrid-capable WSSs, so a superchannel of 275 GHz is configured by the SDN controller. Note that node N6 does not have flex-grid capabilities [32] and, therefore, is discarded for the experiments. At the output of the N4 node there is a 1:8 power splitter and a 25.4 km MCF spool. The power splitter drives the signals to cores 1-8, which correspond to the MCF central core plus 7 adjacent ones. Fibers of different lengths are connecting the 1:8 splitter with the MCF fan-in for decorrelating the signals transmitted in the different cores. The MCF link ends at node N5 (HL2/1), implemented using a 16x16 polymer switch PIC prototype [23] and an OBPF that emulates the output (drop) multicast switch [6]. Note that this node configuration can handle 16 cores and emulate the drop of any channel in the range 191.9 THz - 195.875 THz [25]. So, it can manage up to $16 \times 160 = 2560$ channels with 25 GHz spacing.

The receiver comprises an integrated coherent front-end and a real-time digital oscilloscope (OSC), as described in section 3C. Next the DSP Rx block is in charge of signal downconversion,

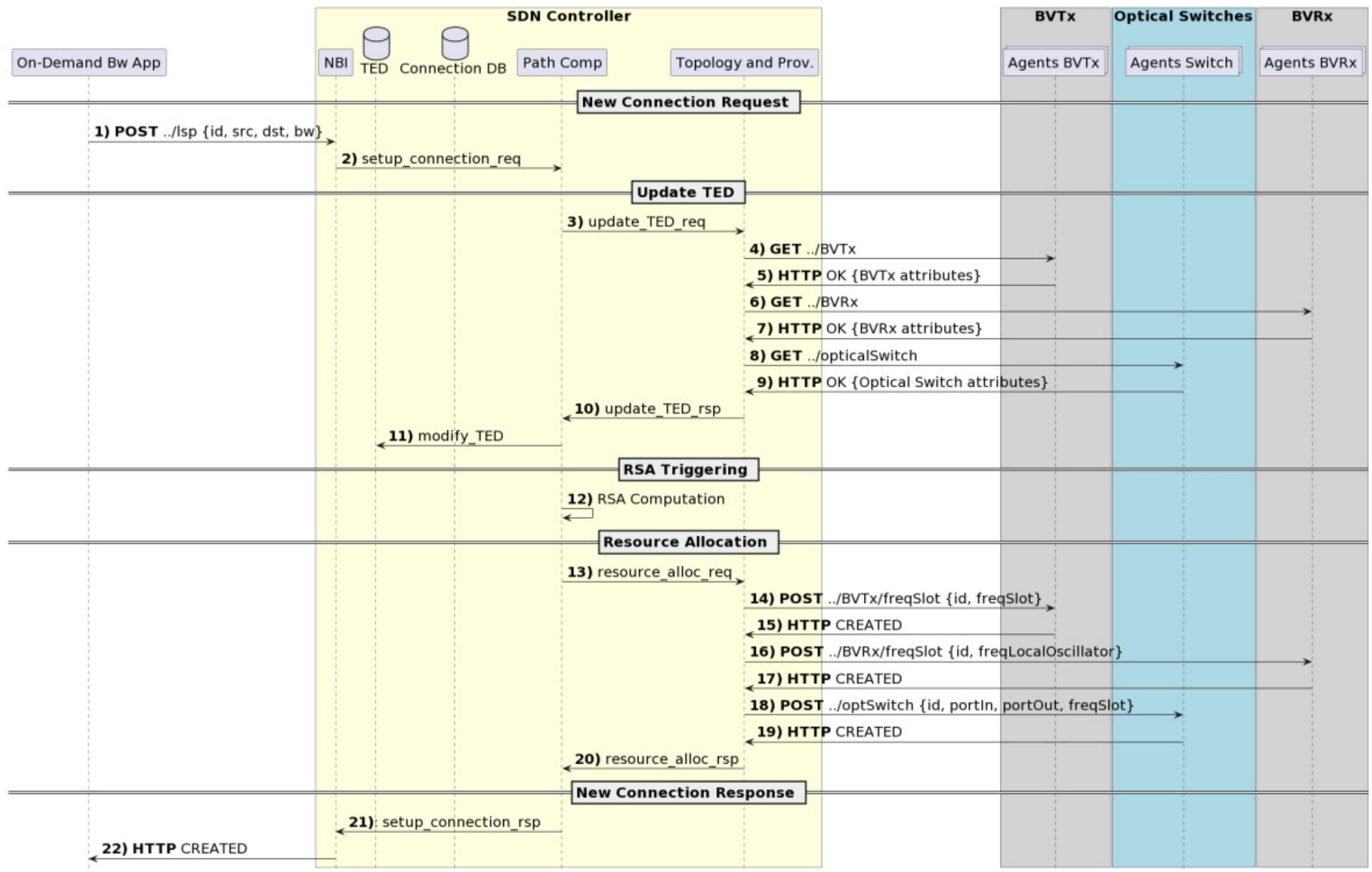

Fig. 8. SDN controlled workflow for setting up a new connection request

equalization and data demodulation, following the steps also detailed in section 3C. This includes dispersion compensation and polarization handling for a reception agnostic to the state of polarization of the received signal.

6. RESULTS

Next, we report the results for the entire network setup. Capacity and BER for the signal under test are summarized in Tab.1. There we can observe that at point B, after passing through the HL4 node, we obtain a capacity of 25.15 Gb/s and 27.72 dB OSNR, in line with back to back results.

At point C, all the dummy channels are aggregated at HL3 node after two hops (15 km), attaining 22.46 Gb/s with OSNR of 26.55 dB, 1.2 dB away from the back to back.

After the HL3 segment, at point D, the accumulated distance is 85 km, covering 4 hops. There we obtain 21.5 Gb/s and 25.43 dB OSNR (∼1 dB penalty with respect to the back to back).

Finally, at point F we obtain 19.05 Gb/s and 24.19 dB OSNR. This is 1.1 dB away from the back to back. At this point, deactivating the dummy channels, we obtain 21.13 Gb/s and $2.9{\cdot}10^{-3}$ BER, which is again in line with the back to back performance. Hence, as expected, previously measured penalties can be mainly ascribed to nonlinear impairments due to tight WDM propagation.

Fig.12 shows the screenshot of the protocol analyzer with the messages exchanged between the SDN controller and the corresponding network nodes. There, it can be seen that the setup delay is 60.45 s, while the delete delay is 4.44 s. Also, details from the configuration of the nodes are shown, such as

Table 1. Capacity and BER for the signal under test at each point of the setup.

Point	Distance	Capacity	BER	OSNR
B	10 km	25.15 Gb/s	$3.4{\cdot}10^{-3}$	27.72 dB
C	15 km	22.46 Gb/s	$4.2{\cdot}10^{-3}$	26.55 dB
D	85 km	21.5 Gb/s	$3.9{\cdot}10^{-3}$	25.43 dB
F	110 km	19.05 Gb/s	$4.5{\cdot}10^{-3}$	24.19 dB

the central frequency (n=198, 194.34 THz) and the bandwidth (m=22, 275 GHz).

7. CONCLUSIONS

Disaggregation and suitable photonic technologies enabling dense integration and programmability are key for future-proof sustainability and scalability of the MAN architecture. In this work, we have assessed the capability of the proposed disaggregated MAN architecture, illustrating the hierarchical network concept, the novel photonic devices and technologies adopted as well as the different network elements, including VCSEL-based S-BVT and switching nodes, and control aspects. We have experimentally assessed a disaggregated metro area network able to handle up to 16×160 = 2560 spatial/spectral channels at different aggregation levels and granularities. An S-BVT based on directly modulated VCSELs and coherent reception is

Fig. 9. JSON-encoded data model: a) the request of a new connection service; b) connection ID and frequency slots; c) frequency of the local oscillator; and d) the message body.

demonstrated to successfully transmit 8×11=88 spatial/spectral channels running at up to 19.05 Gb/s over this infrastructure, covering 110 km and achieving a total capacity of 1.676 Tb/s. This paves the way towards a sustainable dynamic multi-Tb/s connectivity over the MAN for the efficient support of 5G deployment and future 6G services.

FUNDING

Work funded by the H2020 EU PASSION project (G.A. 780326), the ES RELAMPAGO project (PID2021-127916OB-I00), and the ES 6G-OPTRAN-STEROID project (TSI-063000-2021-115).

REFERENCES

1. E. Riccardi, P. Gunning, O. s. G. l. de Dios, M. Quagliotti, V. Lopez, and A. Lord, "An Operator view on the Introduction of White Boxes into Optical Networks," J. Light. Technol. **36**, 3062–3072 (2018).
2. *Europe's age of light! How photonics will power growth and innovation. Strategic Roadmap 2021–2027* (Photonics21, 2019).
3. M. S. Moreolo, J. M. Fabrega, L. Nadal, R. Martinez, and R. Casellas, "Synergy of photonic technologies and software-defined networking in the hyperconnectivity era," J. Light. Technol. **37**, 3902–3910 (2019).
4. "H2020 PASSION Project Factsheet," (2018).
5. N. Tessema, G. Delrosso, S. Bhat, K. Prifti, A. Rasoulzadehzali, R. Stabile, and N. Calabretta, "Modularly and Hybrid Integrated SiPh/InP Wavelength Blocker Switch for Metro Networks," in *2020 European Conference on Optical Communications (ECOC),* (2020), pp. 1–4.
6. N. Tessema, K. Prifti, B. Pan, R. Stabile, and N. Calabretta, "A Novel Modular ROADM Node with Traffic Aggregation/Disaggregation for Ultra-High Capacity SDM Metro Networks," in *2018 European Conference on Optical Communication (ECOC),* (2018), pp. 1–3.
7. A. Malacarne, M. Dallaglio, G. Meloni, N. Sambo, A. Bogoni, C. Neumeyr, L. Poti, and P. Castoldi, "Software-defined reconfigurable vcsel-based transmission," Opt. Express **26**, 9095–9106 (2019).
8. R. Martínez, R. Casellas, M. S. Moreolo, J. M. Fabrega, R. Vilalta, R. Muńoz, L. Nadal, and J. P. Fernández-Palacios, "Proof-of-concept validation of sdn-controlled vcsel-based s-bvts in flexi-grid optical metro networks," in *Optical Fiber Communication Conference (OFC) 2019,* (Optica Publishing Group, 2019), p. W1G.5.
9. J. M. Fabrega, F. J. Vílchez, M. S. Moreolo, R. Martínez, A. Quispe, L. Nadal, R. Casellas, R. Vilalta, R. M. noz, C. Neumeyr, S. Y. Lee, J. U. Shin, H. D. Jung, G. Mariani, R. Heuvelmans, A. Gatto, P. Parolari, P. Boffi, N. M. Tessema, N. Calabretta, D. Larrabeiti, and J. P. Fernández-Palacios, "Experimental demonstration of a metro area network with terabit-capable sliceable bitrate variable transceiver using direct modulated vcsels and coherent detection," in *Optical Fiber Communication Conference (OFC) 2022,* (Optica Publishing Group, 2022), p. M4F.4.
10. J. Wei, Q. Cheng, R. V. Penty, I. H. White, and D. G. Cunningham, "400 gigabit ethernet using advanced modulation formats: Performance, complexity, and power dissipation," IEEE Commun. Mag. **53**, 182–189 (2015).
11. M. Muller, W. Hofmann, T. Grundl, M. Horn, P. Wolf, R. D. Nagel, E. Ronneberg, G. Bohm, D. Bimberg, and M.-C. Amann, "1550-nm high-speed short-cavity vcsels," IEEE J. Sel. Top. Quantum Electron. **17**, 1158–1166 (2011).
12. G. Shen, Y. Zhang, X. Zhou, Y. Sheng, N. Deng, Y. Ma, and A. Lord, "Ultra-dense wavelength switched network: A special eon paradigm for metro optical networks," IEEE Commun. Mag. **56**, 189–195 (2018).
13. C. Wagner, A. Dochhan, M. H. Eiselt, K. Grobe, M. Ortsiefer, C. Gréus, C. Neumeyr, S. Paul, J. Cesar, F. Küppers, J. J. V. Olmos, and I. T. Monroy, "26-gb/s dmt transmission using full c -band tunable vcsel for converged pons," IEEE Photonics Technol. Lett. **29**, 1475–1478 (2017).
14. C. Xie, P. Dong, S. Randel, D. Pilori, P. Winzer, S. Spiga, B. Kögel, C. Neumeyr, and M.-C. Amann, "Single-vcsel 100-gb/s short-reach system using discrete multi-tone modulation and direct detection," in *2015 Optical Fiber Communications Conference and Exhibition (OFC),* (2015), pp. 1–3.
15. C. Xie, S. Spiga, P. Dong, P. J. Winzer, A. Gnauck, C. Gréus, C. Neumeyr, M. Ortsiefer, M. Müller, and M. Amann, "Generation and transmission of 100-Gb/s PDM 4-PAM using directly modulated VCSELs and coherent detection," in *Optical Fiber Communication Conference,* (Optical Society of America, 2014), pp. Th3K–2.
16. S. Paul, C. Gierl, J. Cesar, Q. T. Le, M. Malekizandi, B. Kögel, C. Neumeyr, M. Ortsiefer, and F. Küppers, "10-gb/s direct modulation of widely tunable 1550-nm mems vcsel," IEEE J. Sel. Top. Quantum Electron. **21**, 436–443 (2015).
17. D. M. Marom and M. Blau, "Switching solutions for WDM-SDM optical networks," IEEE Commun. Mag. **53**, 60–68 (2015).
18. S. Sarmiento, J. A. Altabas, D. Izquierdo, I. Garces, S. Spadaro, and J. A. Lazaro, "Cost-effective dwdm roadm design for flexible sustainable optical metro–access networks," J. Opt. Commun. Netw. **9**, 1116–1124 (2017).
19. Y. Ding, V. Kamchevska, K. Dalgaard, F. Ye, R. Asif, S. Gross, M. J. Withford, M. Galili, T. Morioka, and L. K. Oxenløwe, "Reconfigurable sdm switching using novel silicon photonic integrated circuit," Sci. Reports **6**, 1–10 (2016).
20. M. Garrich, E. Magalhães, H. Carvalho, N. G. Gonzalez, G. Zervas, D. Simeonidou, and J. R. Oliveira, "Experimental demonstration of function programmable add/drop architecture for roadms," J. Opt. Commun. Netw. **7**, A335–A343 (2015).
21. T. Goh, M. Yasu, K. Hattori, A. Himeno, M. Okuno, and Y. Ohmori, "Low loss and high extinction ratio strictly nonblocking 16/spl times/16 thermooptic matrix switch on 6-in wafer using silica-based planar lightwave circuit technology," J. lightwave technology **19**, 371–379 (2001).
22. R. M. G. Kraemer, F. Nakamura, Y. Wang, H. Tsuda, and N. Calabretta, "High extinction ratio and low crosstalk c and l-band photonic integrated wavelength selective switching," in *2020 22nd International Conference on Transparent Optical Networks (ICTON),* (2020), pp. 1–4.
23. H.-D. Jung, J.-U. Shin, S.-H. Park, Y.-T. Han, S.-Y. Lee, and Y. Baek, "Polymer-based optical switch for future metro-area networks," in *OSA Advanced Photonics Congress (AP) 2020 (IPR, NP, NOMA, Networks, PVLED, PSC, SPPCom, SOF),* (Optica Publishing Group, 2020), p. PsTh3F.2.
24. "PASSION D2.2 Overall network architecture and control aspects definition," (2020).
25. M. S. Moreolo, J. M. Fabrega, L. Nadal, R. Martinez, R. Casel-

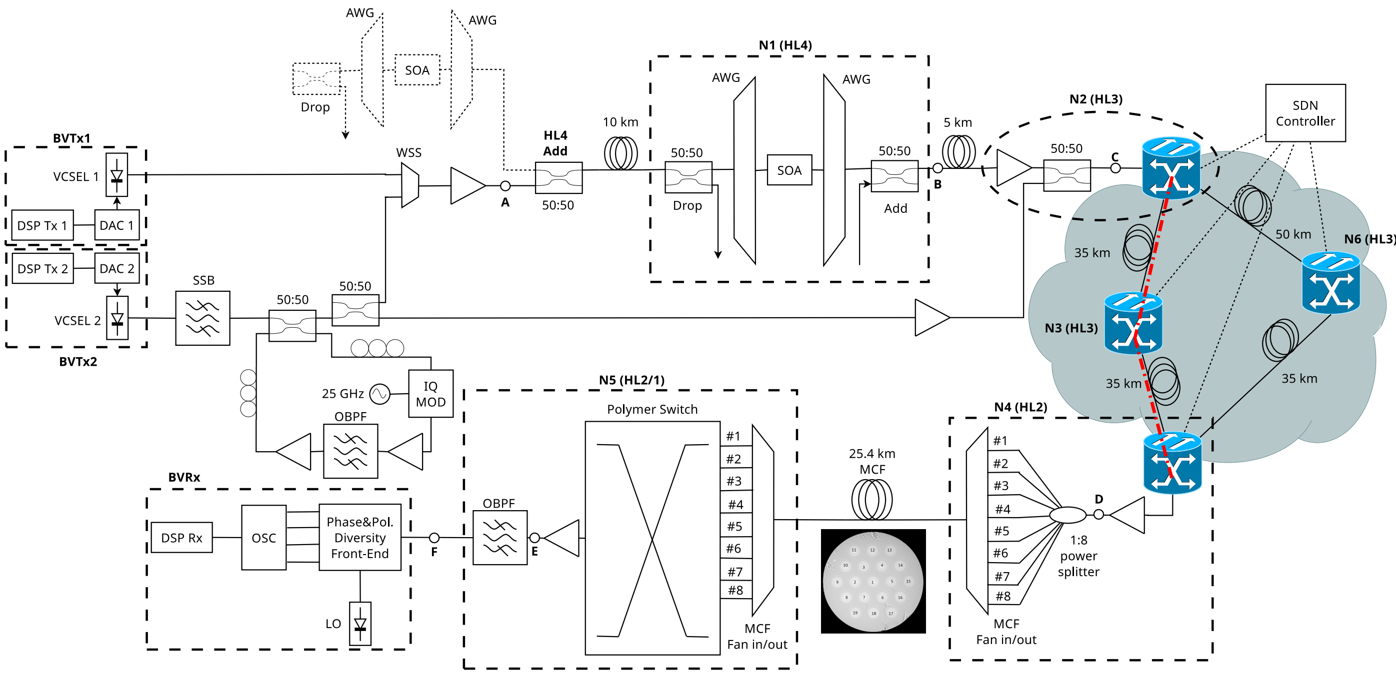

Fig. 10. Experimental setup.

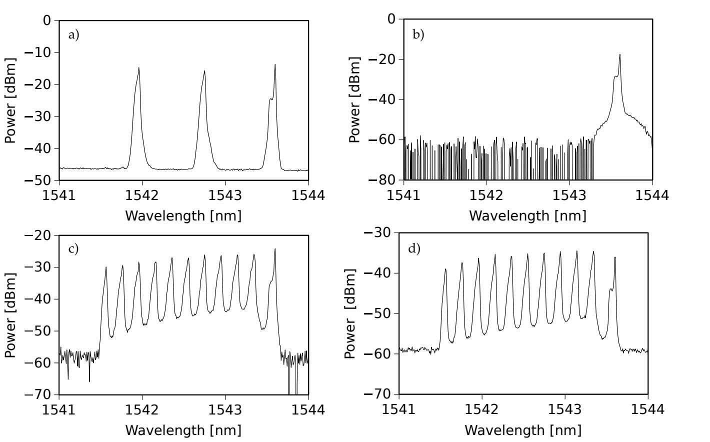

Fig. 11. Spectra at points A (a), B (b), C (c) and E (d)

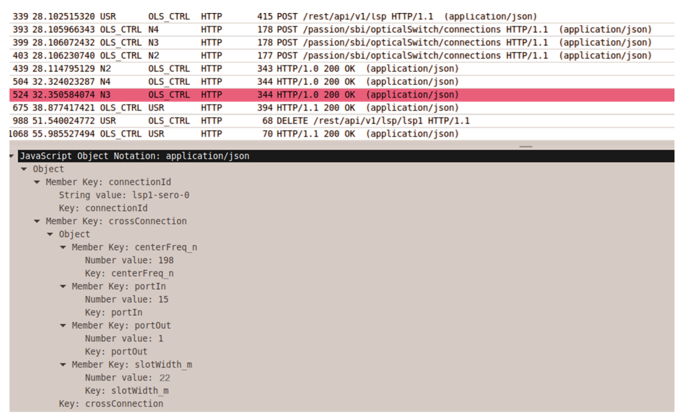

Fig. 12. Wireshark of the configuration of the network nodes.

las, J. Vilchez, R. Munoz, R. Vilalta, A. Gatto, P. Parolari, P. Boffi, C. Neumeyr, D. Larrabeiti, G. Otero, and J. P. Fernandez-Palacios, "Programmable vcsel-based photonic system architecture for future agile tb/s metro networks," J. Opt. Commun. Netw. **13**, A187–A199 (2021).

26. L. Nadal, M. Svaluto Moreolo, J. M. Fàbrega, A. Dochhan, H. Grießer, M. Eiselt, and J.-P. Elbers, "DMT modulation with adaptive loading for high bit rate transmission over directly detected optical channels," J. Light. Technol. **32**, 3541–3551 (2014).
27. "PASSION D4.6 Second generation of hardware efficient modular coherent receivers," (2020).
28. "ITU-T recommendation G.975.1 (2004)," .
29. R. Martínez, R. Casellas, M. S. Moreolo, J. M. Fabrega, R. Vilalta, R. M. noz, L. Nadal, V. López, and J. P. Fernández-Palacios, "Experimental evaluation of an on-line rsa algorithm for sdn-controlled optical metro networks with vcsel-based s-bvts," in *2020 International Conference on Optical Network Design and Modeling (ONDM),* (IEEE, 2020).
30. M. S. Moreolo, R. Martínez, J. M. Fabrega, R. Casellas, J. Vilchez, L. Nadal, R. Vilalta, R. M. noz, C. Neumeyr, H. D. Jung, J. U. Shin, A. Gatto, P. Parolari, P. Boffi, D. Larrabeiti, and J. P. Fernández-Palacios, "Demonstration of an sdn-enabled vcsel-based photonic system for spectral/spatial connectivity in disaggregated optical metro networks," in *Optical Fiber Communication Conference (OFC) 2021,* (Optica Publishing Group, 2021), p. M1B.1.
31. S. Chandrasekhar and X. Liu, "Terabit superchannels for high spectral efficiency transmission," in *36th European Conference and Exhibition on Optical Communication,* (IEEE, Torino, Italy, 2010), pp. 1–6.
32. R. Muñoz, L. Nadal, R. Casellas, M. S. Moreolo, R. Vilalta, J. M. Fàbrega, R. Martínez, A. Mayoral, and F. J. Vílchez, "The adrenaline testbed: An sdn/nfv packet/optical transport network and edge/core cloud platform for end-to-end 5g and iot services," in *2017 European Conference on Networks and Communications (EuCNC),* (2017), pp. 1–5.